Robotica (2008) volume 26, pp. 75–84. © 2007 Cambridge University Press
doi:10.1017/S0263574707003608 Printed in the United Kingdom

Distributed control of modular and reconfigurable robot with torque sensing

Guangjun Liu*†, Sajan Abdul† and Andrew A. Goldenberg‡

†*Department of Aerospace Engineering, Ryerson University, Canada.*
‡*Department of Mechanical and Industrial Engineering, University of Toronto, Canada.*

(Received in Final Form: May 18, 2007. First published online: June 22, 2007)

SUMMARY
A major technical challenge in controlling modular and reconfigurable robots is associated with the kinematics and dynamic model uncertainties caused by reconfiguration. In parallel, conventional model uncertainties such as uncompensated joint friction still persist. This paper presents a modular distributed control technique for modular and reconfigurable robots that can instantly adapt to robot reconfigurations. Under the proposed control method that is based on joint torque sensing, a modular and reconfigurable robot is stabilized joint by joint, and modules can be added or removed without the need to adjust control parameters of the other modules of the robot. Model uncertainties associated with link and payload masses are compensated using joint torque sensor measurement. The remaining model uncertainties, including uncompensated dynamic coupling and joint friction, are compensated by a decomposition-based robust controller. Simulation results have confirmed the effectiveness of the proposed method.

KEYWORDS: Decomposition-based control; Robust control; Modular and reconfigurable robot; Friction compensation; Joint torque sensing.

1. Introduction

With substantial application potential, especially in aerospace sector, the development of modular and reconfigurable robot (MRR) is one of the most promising research areas in robotics.[1] Three types of MRRs have been reported in the literature: self-assembly, self-configuring, and manual configuring. Self-assembly robots possess the highest level of reconfigurability because they can detach from and attach into a robotic system automatically.[2–5] Self-configuring robots cannot perform self-assembly, but they can perform reconfiguration after a robotic system is assembled with some form of manual assistance. Manual-configuring robots are in fact modular robots that can be reconfigured with some form of manual assistance.[6] A survey of MRR systems is discussed in the publication compiled by Setchi and Lagos.[7]

So far, reconfigurable systems are developed based on an *ad hoc* approach due to lack of general-purpose simulation and control techniques. Though such tools are not available, some groundwork has been done and archived in the literature. The main concept of developing reconfigurable robots is based on the use of modular components as building blocks. For this reason, various modules have been proposed for reconfigurable robots. However, these proposed modules are the traditional mechanical components, i.e., joints and links. While the reported reconfigurable robots may represent excellent mechanical design concepts, the modules of known MRRs are not "modular" from control systems point of view because of the existence of dynamic coupling among the modules, which is left to be dealt with by the controller. Conventional robot control methods are based on known robot configuration and its associated dynamic model, with limited allowable model uncertainties such as unknown payloads.[8–10] Even though in theory, robust control schemes can handle large model uncertainties caused by robot reconfigurations, they are not practical because of the large uncertainty that leads to extremely high feedback gains that cannot implemented due to limited structure rigidity, computer sampling rate, actuator bandwidth and saturation, etc. Innovative design and control methods are in need in order to develop truly modular and reconfigurable robots. Melek and Goldenberg recently proposed a neurofuzzy control approach for MRRs, which uses learning control to compensate unmodeled system dynamics due to reconfiguration.[11] The controller parameters are updated using a skill module that is a part of the higher level of the control system hierarchy. While the effectiveness of this approach has been experimentally demonstrated, a difficulty may limit its practical application, which is associated with the initial stage right after a reconfiguration and before the learning controller has learnt the unmodeled system dynamics. At this stage, the behaviour of the robot is not predictable.

Recent development in MRR control includes a position control scheme of MRR discussed by Melek and Najjaran, with consideration of external disturbance.[12] Varying payload at the end-effector is treated as external disturbance, and a mathematical formulation connecting end-effector tracking error and payload is derived. The dynamic control of MRR using a virtual decomposition-based control approach is discussed by Zhu and Lamarche.[13]

In this paper, a control system architecture is developed for modular and reconfigurable articulated robots that can instantly adapt to robot reconfigurations and can control

* Corresponding author. E-mail: gjliu@ryerson.ca.

the reconfigured robot without having to adjust controller parameters. A joint torque sensor is embedded within each module, and the torque sensor measurement is utilized to automatically compensate for the coupling effect. This concept is built upon published research results on robust control of conventional robot manipulators using joint torque sensors.[14,15] However, the known torque sensor-based approaches use centralized control techniques and are inadequate for control of modular robots, which calls for distributed control for each stand-alone module. The proposed method in this paper stabilizes an MRR joint by joint, rather than controlling the robot as a whole, and distributed control is henceforth implemented.

The rest of the paper is organized as follows: Section 2 outlines the dynamic model with joint torque sensors. The proposed control method is presented in Section 3, and simulation results are presented in Section 4. Concluding remarks are given in Section 5.

2. Dynamic Model Formulation

A. *Model formulation*

We consider an MRR constructed with n modules, and each module is integrated with a rotary joint with a speed reducer and a torque sensor as illustrated in Fig. 1.

Similarly as in Imura *et al.*,[14] we assume:

A1. The rotor is symmetric with respect to the axis of rotation.
A2. The joint flexibility is negligible.
A3. The torque transmission does not fail at the speed reducer, and the inertia between the torque sensor and the speed reducer is negligible.

Consider modular and reconfigurable articulated robots with modules installed in series. Each module provides a rotary joint. The base module is denoted as the first module. Modules close to the first module are named lower modules, and modules close to the end-effector are called upper modules.

For the ith module, we use the following notations:

I_{mi}: moment of inertia of the ith rotor about the axis of rotation;
γ_i: reduction ratio of the speed reducer ($\gamma_i \geq 1$);
q_i: joint angle;

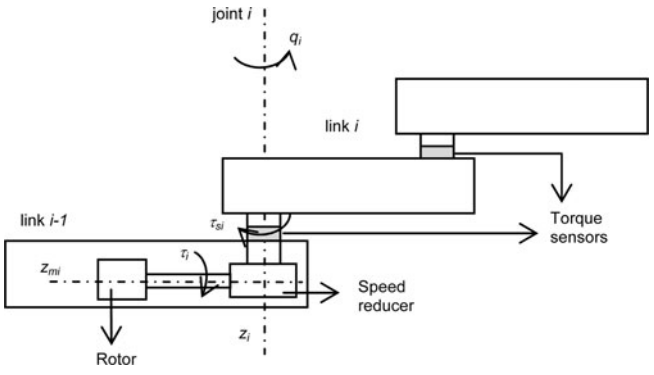

Fig. 1. Schematic diagram of a joint module.

$f_i(q_i, \dot{q}_i)$: joint friction, which is assumed to be a function of the joint position and velocity;[16]
τ_{si}: coupling torque at the torque sensor location;
τ_i: output torque of the rotor;
z_{mi}: unity vector along the axis of rotation of the ith rotor;
z_i: unity vector along the axis of rotation of joint i.

Based on the dynamic equations of a rigid robot manipulator with n rotary joints and joint torque sensing derived by Imura *et al.*,[14] we formulate the dynamic equation of each module. A linearized parametric friction model proposed by Liu[16] is adopted here as discussed later in this section.

For the base module, $i = 1$

$$I_{m1}\gamma_1\ddot{q}_1 + f_1(q_1, \dot{q}_1) + \frac{\tau_{s1}}{\gamma_1} = \tau_1 \tag{1}$$

For the second module from the base, $i = 2$

$$I_{m2}\gamma_2\ddot{q}_2 + f_2(q_2, \dot{q}_2) + I_{m2}z_{m2}^T z_1\ddot{q}_1 + \frac{\tau_{s2}}{\gamma_2} = \tau_2 \tag{2}$$

For $i \geq 3$

$$I_{mi}\gamma_i\ddot{q}_i + f_i(q_i, \dot{q}_i) + I_{mi}\sum_{j=1}^{i-1} z_{mi}^T z_j\ddot{q}_j + I_{mi}\sum_{j=2}^{i-1}\sum_{k=1}^{j-1} z_{mi}^T(z_k \times z_j)\dot{q}_k\dot{q}_j + \frac{\tau_{si}}{\gamma_i} = \tau_i \tag{3}$$

The joint friction $f_i(q_i, \dot{q}_i)$ is assumed to be a function of the joint position and velocity[17,18]

$$f_i(q_i, \dot{q}_i) = \left(f_{ci} + f_{si}\exp\left(-f_{\tau i}\dot{q}_i^2\right)\right)\mathrm{sgn}(\dot{q}_i) + b_i\dot{q}_i + f_{qi}(q_i, \dot{q}_i) \tag{4}$$

where f_{ci} denotes the Coulomb friction-related parameter; f_{si} denotes the static friction-related parameter; $f_{\tau i}$ is a positive parameter corresponding to the Stribeck effect; b_i denotes the viscous friction coefficient; $f_{qi}(q_i, \dot{q}_i)$ reflects the position dependency of friction and other friction modeling errors. The sign function is defined as

$$\mathrm{sgn}(\dot{q}_i) = \begin{cases} 1 & for\ \dot{q}_i > 0 \\ 0 & for\ \dot{q}_i = 0 \\ -1 & for\ \dot{q}_i < 0 \end{cases} \tag{5}$$

The dynamic model is formulated to include Coulomb friction, static friction, Stribeck effect, position dependency, and other bounded disturbances. In this model, frictional memory and rising static friction as discussed by Armstrong *et al.* are assumed negligible.[17] The friction model parameters b_i, f_{ci}, f_{si}, and $f_{\tau i}$ are not accurately known, and they are not necessarily constant. However, their nominal values are determined offline as constants. The nominal values of b_i, f_{ci}, f_{si}, and $f_{\tau i}$ are denoted as $\hat{b}_i$, $\hat{f}_{ci}$, $\hat{f}_{si}$, and $\hat{f}_{\tau i}$, respectively.

https://doi.org/10.1017/S0263574707003608 Published online by Cambridge University Press

The nonparametric friction term $f_{qi}(q, \dot{q})$ is bounded as

$$|f_{qi}(q_i, \dot{q}_i)| < \rho_{fi} \tag{6}$$

where ρ_{fi} is a known constant bound for any position and velocity q_i and $\dot{q}_i$.

B. Model uncertainty analysis

In this section, we examine the parameters and variables in the dynamic equation (3) to identify the model uncertainties and their characteristics. The moment of inertia of the ith rotor about its axis of rotation, I_{mi}, is a physical parameter of the ith module, which can be identified offline and does not vary with the robot reconfiguration. The joint friction is one of the major sources of model uncertainty. The robust friction compensation scheme proposed by Liu[16] will be used in this work to achieve precise control in the presence of joint friction model uncertainty.

Model uncertainty in the third term of Eq. (3), $I_{mi} \sum_{j=1}^{i-1} z_{mi}^T z_j \ddot{q}_j$, can result from the robot reconfiguration, such as misalignment of the axes. The magnitude of this model uncertainty is also dependent upon the accelerations of the first $i-1$ joints. Model uncertainty in the fourth term of Eq. (3), $I_{mi} \sum_{j=2}^{i-1} \sum_{k=1}^{j-1} z_{mi}^T (z_k \times z_j) \dot{q}_k \dot{q}_j$, can also result from the robot reconfiguration. The magnitude of this model uncertainty is dependent upon the velocities of all of the first $i-1$ joints.

Another source of model uncertainty is the joint torque sensor inaccuracy and noise. They depend on the torque sensor performance and are not dealt with in the analysis, but their effect is studied in the simulations.

3. Control Design

Define the overall control for each joint as

$$\tau_i = \frac{\tau_{si}}{\gamma_i} + u_i, \qquad i = 1, 2, \ldots, n \tag{7}$$

where u_i is a new control input to be determined for the ith joint.

For the first (base) joint, $i = 1$, combining Eq. (7) with Eq. (1) yields

$$I_{m1}\gamma_1 \ddot{q}_1 + f_1(q_1, \dot{q}_1) = u_1. \tag{8}$$

As coupling effect does not exist on the base joint, the control input τ_1 can be obtained using control design techniques for a single joint, such as the decomposition-based robust control scheme.[14,16]

For the second joint, $i = 2$, combining Eq. (7) with Eq. (2) yields

$$I_{m2}\gamma_2 \ddot{q}_2 + f_2(q_2, \dot{q}_2) + I_{m2} z_{m2}^T z_1 \ddot{q}_1 = u_2. \tag{9}$$

The inertial force associated with the acceleration of the first joint is involved in Eq. (9), and model uncertainty exists in $z_{m2}^T z_1$ as a result of reconfiguration. However, as the first joint has been stabilized independently, the acceleration of the first joint must be bounded. Hence, the uncertainty in the term $I_{m2} z_{m2}^T z_1 \ddot{q}_1$ is also bounded, and it is well known that such bounded model uncertainty can be compensated with a robust control scheme.

For $i \geq 3$, substituting Eq. (7) into Eq. (3) yields

$$\begin{aligned} I_{mi}\gamma_i \ddot{q}_i + f_i(q_i, \dot{q}_i) + I_{mi} \sum_{j=1}^{i-1} z_{mi}^T z_j \ddot{q}_j \\ + I_{mi} \sum_{j=2}^{i-1} \sum_{k=1}^{j-1} z_{mi}^T (z_k \times z_j) \dot{q}_k \dot{q}_j = u_i, \end{aligned} \qquad i = 3, 4, \ldots, n \tag{10}$$

Examining Eq. (10), one can find that the motion of the upper joints does not affect the lower joints, which has been compensated using the torque measurement in Eq. (7). However, the motion of the lower joints still affects the upper joints through inertial and Coriolis coupling forces. This can be readily understood by analyzing the dynamic equation of the third joint $i = 3$

$$\begin{aligned} I_{m3}\gamma_3 \ddot{q}_3 + I_{m3} \left[z_{m3}^T z_1 \ddot{q}_1 + z_{m3}^T z_2 \ddot{q}_2 \right] \\ + I_{m3} z_{m3}^T (z_1 \times z_2) \dot{q}_1 \dot{q}_2 + f_3(q_3, \dot{q}_3) = u_3 \end{aligned} \tag{11}$$

Inertial and Coriolis forces associated with the motion of the first and second joints are involved in Eq. (11), and reconfiguration can result in model uncertainties in the terms $z_{m3}^T z_1$, $z_{m3}^T z_2$ and $z_{m3}^T (z_1 \times z_2)$. However, as the first and second joints have been stabilized, the accelerations and velocities of the first and second joints must be bounded. Hence, the uncertainties in $I_{m3}[z_{m3}^T z_1 \ddot{q}_1 + z_{m3}^T z_2 \ddot{q}_2]$ and $I_{m3} z_{m3}^T (z_1 \times z_2) \dot{q}_1 \dot{q}_2$ are also bounded and could be compensated with robust control schemes. Expanding the observation to the general case as in Eq. (10), for the ith joint, the model uncertainties in the terms $I_{mi} \sum_{j=1}^{i-1} z_{mi}^T z_j \ddot{q}_j$ and $I_{mi} \sum_{j=2}^{i-1} \sum_{k=1}^{j-1} z_{mi}^T (z_k \times z_j) \dot{q}_k \dot{q}_j$ are bounded and could be compensated with robust control schemes.

Based on the above observation, it can be concluded that the control input u_i can be designed joint by joint, with the consideration of the bounded model uncertainty due to the motion of the lower joints. This conclusion forms the basis of the proposed control design in this paper.

In theory, a saturation-based robust controller can compensate for the bounded model uncertainty. However, high feedback gain is required in order to achieve high accuracy, which is always limited by hardware issues including unmodeled high-order plant dynamics and sensor measurement noise. The key in practical robust control design is to achieve desired performance with minimum feedback gains. To this end, a decomposition-based control design approach is developed by Liu and Goldenberg.[8–10] The fundamental strategy of the decomposition-based system modeling and control approach is to distinguish between uncertain parameters and variables of different physical types, and to design a separate compensator for each of them, while taking into account each specific physical feature. This approach advocates treating each type of model uncertainty with the most suitable and efficient means, including PID, robust, adaptive, and sensor-based control methods. Robust compensators are used only to compensate for uncertainties that cannot be estimated or measured in real time. The overall controller is generated by a synergetic integration of these compensators.

https://doi.org/10.1017/S0263574707003608 Published online by Cambridge University Press

The decomposition-based control approach is applied to design a robust control scheme for the system under consideration. Examining Eq. (10), if we assume that the joint velocities and accelerations are available, the model uncertainties in the above two terms are all due to the unknown misalignment between the joint and motor axes. However, while it is reasonable to assume that the joint velocities are measurable, it is not practical to assume the measurement of joint accelerations, which is avoided in the proposed control method.

First, the following are defined for the control design

$$\begin{aligned} e &= q - q_d \\ r &= \dot{e} + \lambda e \\ a &= \ddot{q}_d - 2\lambda\dot{e} - \lambda^2 e \end{aligned} \tag{12}$$

where λ is any positive constant.

It is assumed that some of the system parameters are unknown but the inertia of motor I_{mi} is known. It is also assumed that the reference trajectory, its first and second derivatives are bounded.

The following two properties are used in the design of control law:

Property 1: Since z_{mi} and z_i are unit vectors along the direction of rotation of the ith rotor and joint, the resulting vector products are bounded as

$$\left|z_{mi}^T z_j\right| \le 1 \qquad \left|z_{mi}^T (z_k \times z_j)\right| \le 1.$$

Property 2: The acceleration and velocity of a stabilized joint is bounded, i.e., if the ith joint is stabilized

$$|\ddot{q}_i| \le \rho_{Di} \qquad |\dot{q}_i| \le \rho_{Vi}$$

where ρ_{Di} and ρ_{Vi} are known constant bounds.

The friction of the ith joint is compensated using the scheme developed by Liu, where $Y(\dot{q}_i)$ and $\tilde{F}^i$ are defined as[16]

$$\begin{aligned} Y(\dot{q}_i) &= [\dot{q}_i \mathrm{sgn}(\dot{q}_i)\exp(-\hat{f}_{\tau i}\dot{q}_i)\mathrm{sgn}(\dot{q}_i) \\ &\quad -\hat{f}_{si}\dot{q}_i^2 \exp(-\hat{f}_{\tau i}\dot{q}_i)\mathrm{sgn}(\dot{q}_i)] \\ \tilde{F}^i &= [\hat{b}_i - b_i\hat{f}_{ci} - f_{ci}\hat{f}_{si} - f_{si}\hat{f}_{\tau i} - f_{\tau i}]^T \end{aligned} \tag{13}$$

If the parametric uncertainty $\tilde{F}^i$ is considered unknown but constant, this uncertainty can be compensated using an integrator-type compensator. However, in practice, the parametric model uncertainty may not always be constant, due to temperature and lubrication changes.

To incorporate variable parametric model uncertainty compensation, $\tilde{F}^i$ is decomposed as

$$\tilde{F}^i = \tilde{F}_c^i + \tilde{F}_v^i \tag{14}$$

where $\tilde{F}_c^i$ is a constant unknown vector, and $\tilde{F}_v^i$ is variable and bounded as follows

$$\left|\tilde{F}_{vn}^i\right| < \rho_n^i, \qquad n = 1, 2, 3, 4. \tag{15}$$

Applying the approach of decomposition-based control design developed by Liu,[16] an adaptive compensator is designed to compensate the constant parametric uncertainty $\tilde{F}_c^i$, and a robust compensator for $\tilde{F}_v^i$.

For stabilizing the first joint, the following control torque is determined

$$\begin{aligned} \tau_1 &= I_{m1}\gamma_1 a_1 + \frac{\tau_{s1}}{\gamma_1} + \hat{b}_1\dot{q}_1 + \left(\hat{f}_{c1} + \hat{f}_{s1}\exp\left(\hat{f}_{\tau 1}\dot{q}_1^2\right)\right)\mathrm{sgn}(\dot{q}_1) \\ &\quad + u_u^1 + Y(\dot{q}_1)\left(u_{pc}^1 + u_{pv}^1\right) \end{aligned} \tag{16}$$

where I_{m1} is the motor inertia for the first joint, τ_{s1} is the coupling torque at the torque sensor location, $\hat{b}_1$, $\hat{f}_{c1}$, $\hat{f}_{s1}$, $\hat{f}_{\tau 1}$ are the nominal friction parameters, u_u^1 is the term designed to compensate for the nonparametric uncertainty $f_{qi}(q, \dot{q})$. The terms u_{pc}^1 and u_{pv}^1 are designed to compensate for the parametric uncertainty $\tilde{F}_c^i$ and $\tilde{F}_v^i$, respectively. The friction compensation is of the same form for all the joints, and hence, for the ith joint, the compensators u_{pc}^i, u_{pv}^i, and u_u^i are defined by

$$u_u^i = \begin{cases} -\rho_{fi}\dfrac{r_i}{|r_i|} |r_i| > \varepsilon^i \\ -\rho_{fi}\dfrac{r_i}{\varepsilon^i} |r_i| \le \varepsilon^i \end{cases} \tag{17}$$

$$\begin{aligned} u_{pc}^i &= -k\int_0^t Y(\dot{q}_i)^T r_i d\tau \\ u_{pvn}^i &= \begin{cases} -\rho_n^i \dfrac{\zeta_n^i}{|\zeta_n^i|} |\zeta_n^i| > \varepsilon_{pn}^i \\ -\rho_n^i \dfrac{\zeta_n^i}{\varepsilon_{pn}^i} |\zeta_n^i| \le \varepsilon_{pn}^i \end{cases}, \qquad n = 1, 2, 3, 4. \end{aligned} \tag{18}$$

where $\zeta^i = Y(\dot{q}_i)^T r_i$, and ε^i, ε_{pn}^i are positive control parameters.

The term $I_{mi}\sum_{j=1}^{i-1} z_{mi}^T z_j \ddot{q}_j$ in Eq. (10) can be rewritten as

$$\begin{aligned} I_{mi}\sum_{j=1}^{i-1} z_{mi}^T z_j \ddot{q}_j &= -\sum_{j=1}^{i-1}\left[I_{mi}\hat{\theta}_j^i I_{mi}\right]\begin{bmatrix}\ddot{q}_j \\ \tilde{\theta}_j^i \ddot{q}_j\end{bmatrix} \\ &\triangleq -\sum_{j=1}^{i-1} I_j^i D_j^i \end{aligned} \tag{19}$$

where $\hat{\theta}_j^i$ is the dot product of the unit vectors z_{mi} and z_j; and $\tilde{\theta}_j^i$ is the alignment error, given by the difference in dot products of the nominal and actual direction vectors.

To include the variable parametric uncertainty in the term $I_{mi}\sum_{j=1}^{i-1} z_{mi}^T z_j \ddot{q}_j$, D_j^i in Eq. (17) can be decomposed into a constant plus a bounded variable term as

$$D_j^i = D_{jc}^i + D_{jv}^i \tag{20}$$

where the variable term D_{jv}^i is bounded as

$$\left|D_{jv}^i\right| \le \rho_{Dj}. \tag{21}$$

https://doi.org/10.1017/S0263574707003608 Published online by Cambridge University Press

Applying decomposition-based control design, an adaptive compensator u^i_{jc} is designed for the constant uncertainty term D^i_{jc} and a robust compensator u^i_{jv} for the variable part D^i_{jv}

$$u^i_{jc} = -k_2 \int_0^t I^{iT}_j r_i d\tau$$
$$u^i_{jvn} = \begin{cases} -\rho_{Dj} \dfrac{\sigma^i_{jn}}{|\sigma^i_{jn}|} |\sigma^i_{jn}| > \varepsilon^i_{Dn} \\ -\rho_{Dj} \dfrac{\sigma^i_{jn}}{\varepsilon_{pni}} |\sigma^i_{jn}| \le \varepsilon^i_{Dn} \end{cases}, \qquad n = 1, 2 \tag{22}$$

where $\sigma^i_j = I^{iT}_j r_i$ and ε^i_{Dn} is a positive control parameter.

Similarly, for the ith joint, $I_{mi} \sum_{j=2}^{i-1} \sum_{k=1}^{j-1} z^T_{mi}(z_k \times z_j)\dot{q}_k \dot{q}_j$ can be rewritten as

$$\begin{aligned} & I_{mi} \sum_{j=2}^{i-1} \sum_{k=1}^{j-1} z^T_{mi}(z_k \times z_j)\dot{q}_k \dot{q}_j \\ & = -\sum_{j=2}^{i-1} \sum_{k=1}^{j-1} \left[I_{mi} \hat{\Theta}^i_{kj} I_{mi} \right] \begin{bmatrix} \dot{q}_k \dot{q}_j \\ \tilde{\Theta}^i_{kj} \dot{q}_k \dot{q}_j \end{bmatrix} \\ & \triangleq -\sum_{j=2}^{i-1} \sum_{k=1}^{j-1} J^i_{kj} P^i_{kj} \end{aligned} \tag{23}$$

where the term P^i_{kj} can be decomposed as

$$P^i_{kj} = P^i_{kjc} + P^i_{kjv} \tag{24}$$

where the variable term P^i_{kjv} is bounded as

$$\left| P^i_{kjv} \right| \le \rho_{Vk} \rho_{Vj}. \tag{25}$$

Applying decomposition-based control design, an adaptive compensator V^i_{kjc} can be designed for the constant uncertainty term P^i_{kjc} and a robust compensator V^i_{kjv} for the variable part P^i_{kjv}.

The terms V^i_{kjc} and V^i_{kjv} are defined as

$$V^i_{kjc} = -k_3 \int_0^t J^{i\ T}_{kj} r_i d\tau$$
$$V^i_{kjvn} = \begin{cases} -\rho_{Vk}\rho_{Vj} \dfrac{\beta^i_{kjn}}{|\beta^i_{kjn}|} |\beta^i_{kjn}| > \varepsilon^i_{Vn} \\ -\rho_{Vk}\rho_{Vj} \dfrac{\beta^i_{kjn}}{\varepsilon_{pin}} |\beta^i_{kjn}| \le \varepsilon^i_{Vn} \end{cases}, \qquad n = 1, 2 \tag{26}$$

where $\beta^i_{kj} = J^{i\ T}_{kj} r_i$ and ε^i_{Vn} is a positive control parameter.

The stabilization of the first joint, using control law given by Eq. (16), ultimately results in the uniform boundedness of tracking error, and thus, the boundedness of the magnitudes of $\dot{q}_1$ and $\ddot{q}_1$. Since $\ddot{q}_1$ is bounded, a compensator designed using saturation-based robust control could be used to compensate for the effects of $\ddot{q}_1$. Thus, the control torque τ_2 for the second joint would be given by the control law developed by Liu[16] with an additional term $I^2_1(u^2_{1c} + u^2_{1v})$ to compensate for the effects of $\ddot{q}_1$

$$\begin{aligned} \tau_2 = {} & I_{m2}\gamma_2 a_2 + \hat{b}\dot{q}_2 + \left(\hat{f}_c + \hat{f}_s \exp\left(\hat{F}_\tau \dot{q}^2_2 \right) \right) \mathrm{sgn}(\dot{q}_2) + u_{u2} \\ & + I^2_1 \left(u^2_{1c} + u^2_{1v} \right) + Y(\dot{q}_2) \left(u^2_{pc} + u^2_{pv} \right) + \frac{\tau_{s2}}{\gamma_2}. \end{aligned} \tag{27}$$

Similarly for the ith joint, we have control torque τ_i given by

$$\begin{aligned} \tau_i = {} & I_{mi}\gamma_i a_i + \frac{\tau_{si}}{\gamma_i} + \hat{b}\dot{q}_i + \left(\hat{f}_c + \hat{f}_s \exp\left(\hat{f}_\tau \dot{q}^2_i \right) \right) \mathrm{sgn}(\dot{q}_i) \\ & + u_{ui} + Y(\dot{q}_i) \left(u^i_{pc} + u^i_{pv} \right) + \sum_{j=1}^{i-1} I^i_j \left(u^i_{jc} + u^i_{jv} \right) \\ & + \sum_{j=2}^{i-1} \sum_{k=1}^{j-1} J^i_{kj} \left(V^i_{kjc} + V^i_{kjv} \right) \end{aligned} \tag{28}$$

with the last two terms of Eq. (28) corresponding to the compensators for the joint accelerations and velocities of the lower joints.

Substituting Eqs. (19), (23) and Eq. (28) into (10) yields the closed-loop expression for the ith joint as

$$\begin{aligned} M_i \dot{r}_i + \lambda M_i r_i = {} & Y(\dot{q}_i)(\tilde{F}_c + u_{pci}) + Y(\dot{q}_i)(\tilde{F}_v + u_{pvi}) + u_{ui} \\ & - f_{qi}(q_i, \dot{q}_i) + \sum_{j=1}^{i-1} I^i_j \left(u^i_{jc} + u^i_{jv} \right) + \sum_{j=1}^{i-1} I^i_j D^i_j \\ & + \sum_{j=2}^{i-1} \sum_{k=1}^{j-1} J^i_{kj} P^i_{kj} + \sum_{j=2}^{i-1} \sum_{k=1}^{j-1} J^i_{kj} \left(V^i_{kjc} + V^i_{kjv} \right) \end{aligned} \tag{29}$$

where $M_i = I_{mi}\gamma_i$.

Theorem: *Given an n-DOF modular robot, with joint dynamics as given in Eqs. (7–10) and the model uncertainty defined by Eqs. (19) and (23), the tracking error of each joint is ultimately uniformly bounded under the control law defined by Eq. (28). The ultimate bound of the tracking error is determined by the nonparametric uncertainty and control parameters only, and it is not affected by the parametric uncertainty.*

Proof. A Lyapunov function candidate is defined as

$$V = \frac{1}{2} M_i r^2_i + \frac{1}{2} k \Psi^T \Psi + \frac{1}{2} k_2 \Lambda_i{}^T \Lambda_i + \frac{1}{2} k_3 \Omega_i{}^T \Omega_i \tag{30}$$

where $\Psi = \frac{1}{k}\tilde{F}_c - \int_0^t Y(\dot{q}_i)^T r_i d\tau$, $\Lambda_i = \sum_{j=1}^{i-1} (\frac{1}{k_2} D^i_{jc} - \int_0^t I^{iT}_j r_i d\tau)$, and $\Omega_i = \sum_{j=2}^{i-1} \sum_{k=1}^{j-1} (\frac{1}{k_3} P^i_{kjc} - \int_0^t J^{i\ T}_{kj} r_i d\tau)$.

Since k, k_2, k_3 and $\tilde{F}_c$, D^i_{jc}, P^i_{kjc} are constants, $\dot{\Psi}$, $\dot{\Lambda}_i$ and $\dot{\Omega}_i$ are given by $\dot{\Psi} = -Y(\dot{q}_i)^T r_i$, $\dot{\Lambda}_i = -I^{iT}_j r_i$ and $\dot{\Omega}_i =$

https://doi.org/10.1017/S0263574707003608 Published online by Cambridge University Press

$-J_{kj}^{i\,T} r_i$. Differentiating Eq. (30) yields

$$\begin{aligned}\dot{V} &= M r_i \dot{r}_i + k\Psi^T \dot{\Psi} + k\Lambda_i^T \dot{\Lambda}_i + k\Omega_i^T \dot{\Omega}_i \\ &= r_i(-\lambda M_i r_i + Y(\dot{q}_i)(\tilde{F}_c + u_{pci}) + Y(\dot{q}_i)(\tilde{F}_v + u_{pvi}) \\ &\quad + \sum_{j=1}^{i-1} I_j^i\left(u_{jc}^i + u_{jv}^i\right) + \sum_{j=1}^{i-1} I_j^i\left(D_{jc}^i + D_{jv}^i\right) \\ &\quad + \sum_{j=2}^{i-1}\sum_{k=1}^{j-1} J_{kj}^i\left(P_{kjc}^i + P_{kjv}^i\right) + \sum_{j=2}^{i-1}\sum_{k=1}^{j-1} J_{kj}^i\left(V_{kjc}^i + V_{kjv}^i\right) \\ &\quad - k\zeta^T Y(q_i)^T r_i - k_2 \Lambda_i^T I_j^{i\,T} r_i - k_3 \Omega_i^{\,T} P_{kj}^{i\,T} r_i + u_{ui} \\ &\quad - F_{qi}(q_i, \dot{q}_i) \\ &= -\lambda M_i r_i^2 + r_i Y(\dot{q}_i)(\tilde{F}_v + u_{pvi}) + r_i(u_{ui} - F_{qi}(q_i, \dot{q}_i)) \\ &\quad + \sum_{j=1}^{i-1}\left(r_i I_j^i\left(D_{jv}^i + u_{jv}^i\right)\right) + \sum_{j=2}^{i-1}\sum_{k=1}^{j-1} r_i J_{kj}^i\left(P_{kjc}^i + V_{kjv}^i\right)\end{aligned}$$

$$\begin{aligned} r_i Y(\dot{q}_i)\left(\tilde{F}_v + u_{pv}^i\right) &= \sum_{n=1}^{4} r_i Y_n\left(\tilde{F}_{vn} + u_{pvn}^i\right) \\ &= \sum_{n=1}^{4} \zeta_n^i\left(\tilde{F}_{vn} + u_{pvn}^i\right)\end{aligned}$$

For ith joint, and $n = 1, 2, 3, 4$, if $|\zeta_n^i| > \varepsilon_{pn}^i$

$$\zeta_n^i\left(\tilde{F}_{vn} + u_{pvn}^i\right) = \zeta_n^i\left(\tilde{F}_{vn} - \rho_n^i \frac{\zeta_n^i}{|\zeta_n^i|}\right) < 0 \qquad (31)$$

If $|\zeta_n^i| \le \varepsilon_{pn}^i$

$$\begin{aligned}\zeta_n^i\left(F_{vn} + u_{pvn}^i\right) &= \zeta_n^i\left(\tilde{F}_{vn} - \rho_n^i \frac{\zeta_n^i}{|\zeta_n^i|}\right) \\ &\le \zeta_n^i\left(\rho_n^i \frac{\zeta_n^i}{|\zeta_n^i|} - \rho_n^i \frac{\zeta_n^i}{\varepsilon_{pn}^i}\right) \qquad (32)\end{aligned}$$

$$\begin{aligned} r_i I_j^i\left(D_{jv}^i + u_{jv}^i\right) &= \sum_{n=1}^{2} r_i I_j^i\left(D_{jvn}^i + u_{jvn}^i\right) \\ &= \sum_{n=1}^{2} \sigma_{jn}^i\left(D_{jvn}^i + u_{jvn}^i\right)\end{aligned}$$

For ith joint, and $n = 1, 2$, $j = 1 \ldots (i-1)$ if $|\sigma_{jn}^i| > \varepsilon_{Dn}^i$

$$\sigma_{jn}^i\left(D_{jvn}^i + u_{jvn}^i\right) = \sigma_{jn}^i\left(D_{jvn}^i - \rho_{Dj}\frac{\sigma_{jn}^i}{|\sigma_{jn}^i|}\right) < 0 \qquad (33)$$

If $|\sigma_{jn}^i| \le \varepsilon_{Dn}^i$

$$\begin{aligned}\sigma_{jn}^i\left(D_{jvn}^i + u_{jvn}^i\right) &= \sigma_{jn}^i\left(D_{vn} - \rho_{Dn}\frac{\sigma_{jn}^i}{|\sigma_{jn}^i|}\right) \\ &\le \zeta_n^i\left(\rho_{Dn}\frac{\sigma_{jn}^i}{|\sigma_{jn}^i|} - \rho_{Dn}\frac{\sigma_{jn}^i}{\varepsilon_{Dn}^i}\right) \qquad (34)\end{aligned}$$

$$\begin{aligned} r_i J_{kj}^i\left(P_{kjv}^i + V_{kjv}^i\right) &= \sum_{n=1}^{2} r_i J_{kj}^i\left(P_{kjvn}^i + V_{kjvn}^i\right) \\ &= \sum_{n=1}^{2} \beta_{kjn}^i\left(P_{kjvn}^i + V_{kjvn}^i\right)\end{aligned}$$

For ith joint, and $n = 1, 2$, $j = 1 \ldots (i-1)$ if $|\beta_{kjn}^i| > \varepsilon_{Vn}^i$

$$\beta_{kjn}^i\left(P_{kjvn}^i + V_{kjvn}^i\right) = \beta_{kjn}^i\left(P_{kjvn}^i - \rho_{Vj}\rho_{Vk}\frac{\beta_{kjn}^i}{|\beta_{kjn}^i|}\right) < 0 \qquad (35)$$

If $|\beta_{kjn}^i| \le \varepsilon_{Vn}^i$

$$\begin{aligned}\beta_{kjn}^i\left(P_{kjvn}^i + V_{kjvn}^i\right) &= \beta_{kjn}^i\left(P_{vn} - \rho_{Vj}\rho_{Vk}\frac{\beta_{kjn}^i}{|\beta_{kjn}^i|}\right) \\ &\le \beta_n^i\left(\rho_{Vj}\rho_{Vk}\frac{\beta_{kjn}^i}{|\beta_{kjn}^i|} - \rho_{Vj}\rho_{Vk}\frac{\beta_{kjn}^i}{\varepsilon_{Vn}^i}\right). \qquad (36)\end{aligned}$$

Since the last terms of Eqs. (32), (34), and (36) achieve a maximum value at $|\zeta_{jn}^i| \le \varepsilon_{pn}^i/2$, $|\sigma_{jn}^i| \le \varepsilon_{Dn}^i/2$ and $|\beta_{kjn}^i| \le \varepsilon_{Vn}^i/2$ we have

$$\begin{aligned}\dot{V} &\le -\lambda M_i r_i^2 + \frac{\rho\varepsilon_i}{4} + \sum_{j=2}^{i-1}\sum_{k=1}^{j-1}\left(\sum_{n=1}^{2}\frac{\rho_{Vk}\rho_{Vj}\varepsilon_{Vn}}{4}\right) \\ &\quad + \sum_{j=1}^{i-1}\left(\sum_{n=1}^{2}\frac{\rho_{Djn}\varepsilon_{Dn}^i}{4}\right) + \sum_{n=1}^{4}\frac{\rho_n^i\varepsilon_{pn}^i}{4} \qquad (37)\end{aligned}$$

From Eq. (36), it can be concluded that a Lyapunov function can be found only if

$$|r_i| > \sqrt{\frac{\left(\begin{array}{c}\rho\varepsilon_i + \sum_{j=2}^{i-1}\sum_{k=1}^{j-1}\left(\sum_{n=1}^{2}\rho_{Vk}\rho_{Vj}\varepsilon_{Vn}\right) \\ + \sum_{j=1}^{i-1}\left(\sum_{n=1}^{2}\rho_{Djn}\varepsilon_{Dn}^i\right) + \sum_{n=1}^{4}\rho_{in}\varepsilon_{pin}\end{array}\right)}{4\lambda M_i}}.$$

https://doi.org/10.1017/S0263574707003608 Published online by Cambridge University Press

Define

$$S = \left\{ r_i \in R^1 \middle| r_i^2 \right.$$
$$\left. \leq \left(\begin{array}{l} \rho\varepsilon_i + \sum_{j=2}^{i-1} \sum_{k=1}^{j-1} \left(\sum_{n=1}^{2} \rho_{Vk}\rho_{Vj}\varepsilon_{Vn} \right) \\ + \sum_{j=1}^{i-1} \left(\sum_{n=1}^{2} \rho_{Djn}\varepsilon_{Dn}^{i} \right) + \sum_{n=1}^{4} \rho_{in}\varepsilon_{pin} \end{array} \right) \Big/ (2\lambda M_i) \right\}$$

Then, on the surface of S, ∂S, we have

$$\dot{V} \leq -\left(\begin{array}{l} \rho\varepsilon_i + \sum_{j=2}^{i-1} \sum_{k=1}^{j-1} \left(\sum_{n=1}^{2} \rho_{Vk}\rho_{Vj}\varepsilon_{Vn} \right) \\ + \sum_{j=1}^{i-1} \left(\sum_{n=1}^{2} \rho_{Djn}\varepsilon_{Dn}^{i} \right) + \sum_{n=1}^{4} \rho_{in}\varepsilon_{pin} \end{array} \right) \Big/ 4.$$

Denote T as the time for the solution trajectory to intersect the surface ∂S, then

$$V(r_i(T)) - V(r_i(0))$$
$$\leq -\left(\left(\begin{array}{l} \rho\varepsilon_i + \sum_{j=2}^{i-1} \sum_{k=1}^{j-1} \left(\sum_{n=1}^{2} \rho_{Vk}\rho_{Vj}\varepsilon_{Vn} \right) \\ + \sum_{j=1}^{i-1} \left(\sum_{n=1}^{2} \rho_{Djn}\varepsilon_{Dn}^{i} \right) + \sum_{n=1}^{4} \rho_{in}\varepsilon_{pin} \end{array} \right) \Big/ 4 \right) T.$$

Hence

$$T \leq 4\,(V(r_i(T)) - V(r_i(0)))$$
$$\Big/ \left(\begin{array}{l} \rho\varepsilon_i + \sum_{j=2}^{i-1} \sum_{k=1}^{j-1} \left(\sum_{n=1}^{2} \rho_{Vk}\rho_{Vj}\varepsilon_{Vn} \right) \\ + \sum_{j=1}^{i-1} \left(\sum_{n=1}^{2} \rho_{Djn}\varepsilon_{Dn}^{i} \right) + \sum_{n=1}^{4} \rho_{in}\varepsilon_{pin} \end{array} \right).$$

The boundedness of r_i implies the boundedness of e_i and $\dot{e}_i$ as per the proof developed by Slotine and Li.[19]

4. Simulations

A. Dynamic model

To study the effectiveness of the proposed control scheme, a 3-DOF planar robot, working in a horizontal plane with the following parameters is used to conduct simulations

$$\begin{aligned} b_i &= 1.5 + 0.3\sin(10q_i)\ \text{Nm s/rad}, \\ f_{ci} &= 3.5 + 0.7\sin(10q_i)\ \text{Nm}, \\ f_{si} &= 5 + \sin(10q_i)\ \text{Nm}, \\ f_{\tau i} &= 100 + 20\sin(10q_i)\ \text{s}^2/\text{rad}^2. \end{aligned}$$

Table 1. Parameters of the simulated system.

	Link 1	Link 2	Link 3
Mass of link (kg)	8	5	4
Length of link (m)	1	1	1
Link inertia (kgm^2)	1.0	0.8	0.6
Distance to center of mass (m)	0.5	0.5	0.5
Rotor inertia (kgm^2)	0.4	0.2	0.1
Gear reduction ratio	100	100	100

The dynamic equations of the manipulator are given in the Appendix. For the simulations, the parameters of the manipulator are chosen as in Table I.

The parametric uncertainty bounds are determined to be

$$\begin{aligned} &\rho_1^i = 0.3\,\text{Nm s/rad} \quad \rho_2^i = 1\,\text{Nm} \\ &\rho_3^i = 0.7\,\text{Nm} \quad \rho_4^i = 20\,\text{s}^2/\text{rad}^2 \\ &\lambda = 100 \quad k = 1 \quad k_2 = 1 \quad k_3 = 1 \quad \varepsilon^i = 0.1 \\ &\varepsilon_{p1}^i = 0.01 \quad \varepsilon_{p2}^i = 0.01 \quad \varepsilon_{p3}^i = 0.01 \quad \varepsilon_{p4}^i = 0.01 \\ &\varepsilon_{V1}^3 = 0.01 \quad \varepsilon_{V2}^3 = 0.01 \quad \varepsilon_{D1}^i = 0.01 \quad \varepsilon_{D2}^i = 0.01 \end{aligned} \tag{38}$$

The nominal parameters of the friction model are

$$\hat{b}_i = 1.2\,\text{Nm s/rad}, \quad \hat{f}_{si} = 4\,\text{Nm}, \quad \hat{f}_{i\tau} = 80\,\text{s}^2/\text{rad}^2,$$
$$\hat{f}_{ic} = 3.0\,\text{Nm}$$

and the position dependent friction is realized as $F_q(q, \dot{q}) = 0.5\sin(3q)$, with the uncertainty bound $\rho_{fi} = 0.5$. For simplicity, the same friction model and parameters were considered for all the three joints.

The desired trajectories for the three joints are selected as

$$q_{d1} = 1 - \cos(\pi t/3), \quad q_{d2} = 1 - \cos(\pi t/3),$$
$$q_{d3} = 1 - \cos(\pi t/3)$$

for $0 \leq t \leq 18$ s.

B. Simulation results

Applying the control law in Eq. (26) to the 3-DOF modular robot defined by Eqs (8), (9), and (11) and with parametric bounds given by Eq. (38), we obtain the results shown in Fig. 2, depicting the position tracking errors of the three joints. A small increase in tracking errors at the upper joints is observed, which can be attributed to the disturbance from the stabilized lower joints. This scenario can be distinctly noted by using the same reference trajectory for all the three joints.

To study the tracking error variation with sensor dynamics, simulations are carried out for different values of linearity and ripple factors of the torque sensor. The effect of ripple on tracking errors is studied, with the resulting error plot for the third joint shown in Fig. 3. The 5% ripple on torque sensor is compared against a 0% ripple. A nonlinearity of 5% of full scale is compared with the results for a sensor with zero nonlinearity, and the resulting tracking error of the first joint is shown in Fig. 4. In the simulations, 200 Nm was considered to be the full scale torque value. Since practical torque sensors have a delay in signal transmission, simulations were also carried with torque sensor delays. The tracking performance of the first joint in the presence of delay in the torque sensor

https://doi.org/10.1017/S0263574707003608 Published online by Cambridge University Press

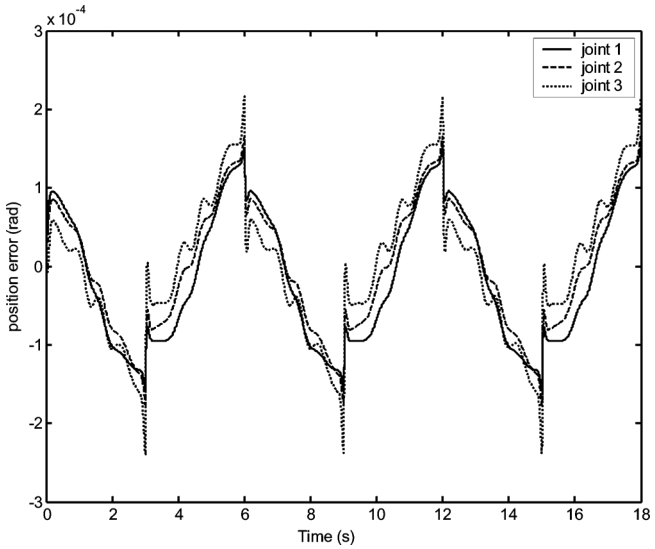

Fig. 2. Position tracking errors of three joints.

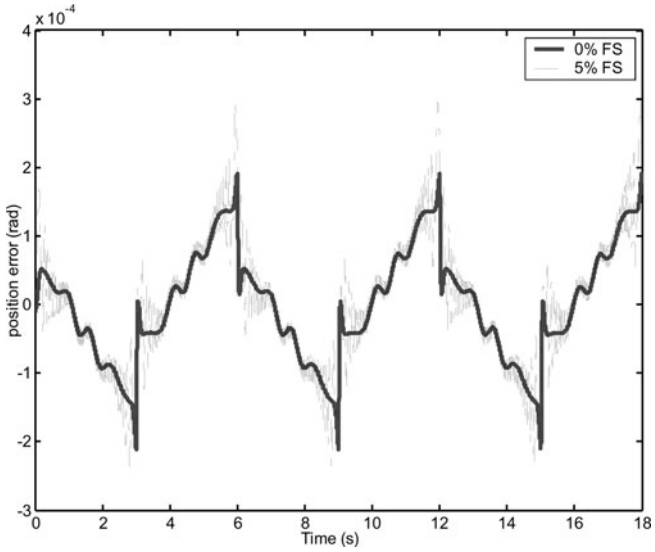

Fig. 3. Position error of the third joint with torque sensor ripples.

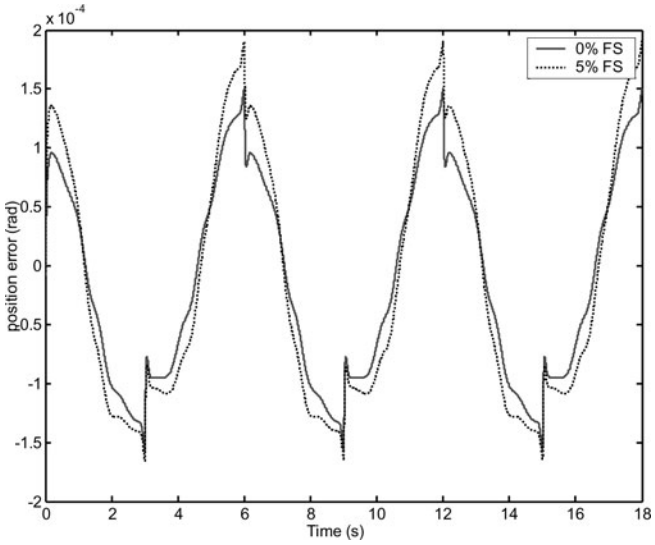

Fig. 4. Position error of the first joint with torque sensor nonlinearity.

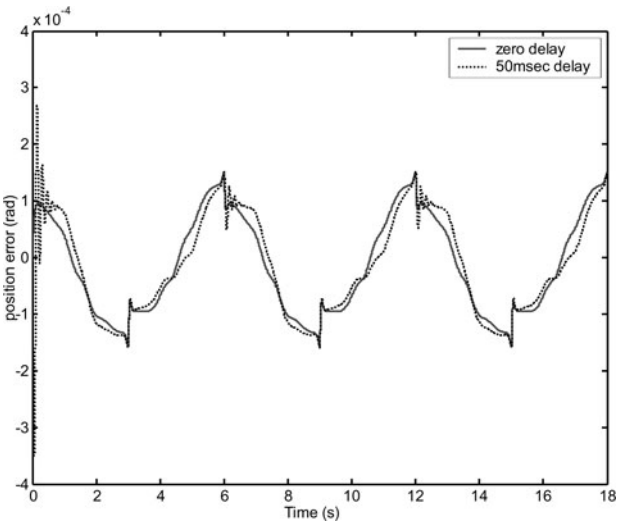

Fig. 5. Position error of the first joint with torque sensor delay.

signal is shown in Fig. 5. The controller was observed to be able to compensate for the errors due to the sensor delay. The tracking errors for the other joints showed similar trends under the above considered ripple, nonlinearity, and sensor delay values.

It is seen that lower tracking errors are obtained for lower values of ripple factor and lower nonlinearity factors. For larger time delays, it is seen that the tracking errors are higher due to additional time lags introduced by the sensor delay. During the simulations, it was observed that with higher gear ratio, the effects of torque sensor nonlinearities can be reduced as expected.

5. Conclusions

A new distributed control approach to design and control MRRs is proposed based on joint torque sensing. Under the proposed control system architecture, an MRR is stabilized joint by joint, and modules can be added or removed without the need to adjust control parameters. Model uncertainties associated with link and payload masses are compensated using joint torque sensor measurement, and the remaining model uncertainties including unmodeled dynamic coupling effect and joint friction are compensated by a decomposition-based robust controller. The effect of sensor dynamics on the control scheme is studied with torque ripple, sensor delay, and sensor nonlinearities under consideration. The proposed controller is robust against the dynamic effects of the torque sensor. Simulation results have confirmed the effectiveness of the proposed approach.

Acknowledgment

This work is supported in part by a Collaborative Research and Development (CRD) grant by Natural Sciences and Engineering Research Council (NSERC) of Canada, Engineering Services Inc., and the Canadian Space Agency.

References

1. M. Yim, W.-M. Shen, B. Salemi, D.Rus, M. Moll, H. Lipson, E. Klavins and G. S. Chirikjian, “Modular self-reconfigurable

https://doi.org/10.1017/S0263574707003608 Published online by Cambridge University Press

robot systems—Challenges and opportunities for future," *IEEE Robot. Autom. Mag.* **14**(1), 43–52 (2007).
2. T. Fukuda and S. Nakagawa, "Dynamically Reconfigurable Robotic System," *Procedings of the IEEE International Conference on Robotics and Automation* **3** (1988) pp. 1581–86.
3. G. Chirikjian, "Kinematics of a Metamorphic Robotic System,"*Proceedings IEEE International Conference Robotics and Automation* **1** (1994) pp. 449–55.
4. M. Yim, D. G. Duff and K. D. Roufas, "Polybot: A Modular Reconfigurable Robot," *Proceedings IEEE International Conference Robotics and Automation* **1** (2000) pp. 514–20.
5. K. Tomita, S. Murata, E. Yoshida, H. Kurokawa and S. Kokaji, "Reconfiguration method for a distributed mechanical system," *Distrib. Autonom. Robot. Syst.* **2**, 17–25 (1996).
6. R. Hui, N. Kircanski, A. A. Goldenberg, C. Zhou, P. Kuzan, J. Wiercienski, D. Gershon and P. Sinha, "Design of the IRIS Facility—A Modular, Reconfigurable and Expandable Robot Test Bed," *Proceedings IEEE International Conference on Robotics and Automation* **3** (1993) pp. 155–60.
7. R. M. Setchi and N. Lagos, "Reconfigurability and Reconfigurable Manufacturing Systems: State-of-the-Art Review," *Proceedings IEEE International Conference of Industrial Informatics* (2004) pp. 529–35.
8. G. Liu and A. A. Goldenberg, "Robust control of robot manipulators based on dynamics decomposition," *IEEE Trans. Robot. Autom.* **13**(5), 783–89 (1997).
9. G. Liu and A. A. Goldenberg, "Uncertainty decomposition-based robust control of robot manipulators," *IEEE Trans. Control Sys. Technol.* **4**(4), 384–93 (1996).
10. G. Liu and A. A. Goldenberg, "Comparative study of robust saturation control of robot manipulators: Analysis and experiments," *Int. J. Robot. Res.* **15**(5), 473–91 (1996).
11. W. W. Melek and A. A. Goldenberg, "Neurofuzzy control of modular and reconfigurable robots," *IEEE/ASME Trans. Mech.* **8**(3), 381–89 (2003).
12. W. W. Melek and H. Najjaran, "Study of the Effect of External Disturbances on the Position Control of IRIS Modular and Reconfigurable Manipulator," *IEEE International Conference on Mechatronics and Automation*, 144–147 (2005).
13. W.-H. Zhu and T. Lamarche, "Modular Robot Manipulators Based on Virtual Decomposition Control," *Proceedings IEEE International Conference Robotics and Automation*, Roma, Italy, (2007) pp. 2235–2240.
14. J. Imura, T. Sugie, Y. Yokokohji and T. Yoshikawa, "Robust Control of Robot Manipulators Based on Joint Torque Sensor Information," *Proceedings of IEEE/RSJ International Workshop on Intelligent Robots and Systems, Osaka, Japan,* (1991) pp. 344–349.
15. K. Kosuge, H. Takeuchi and K. Furuta, "Motion control of a robot arm using joint torque sensors," *IEEE Trans. Robot. Autom.* **6**(2), 258–263 (1990).
16. G. Liu, "Decomposition-based friction compensation of mechanical systems," *Mechatronics* **12**(5), 755–769 (2002).
17. B. Armstrong-Helouvry, P. Dupont and C. Canudas de Wit, "A survey of models, analysis tools and compensation methods for the control of machines with friction," *Automatica* **30**(7), 1083–1138 (1994).
18. G. Liu, A. A. Goldenberg and Y. Zhang, "Precise slow motion control of a direct-drive robot arm with velocity estimation and friction compensation," *Mechatronics* **14**(7), 821–834 (2004).
19. J. J. E. Slotine and W. Li, *Applied nonlinear control* (Prentice-Hall, Englewood Cliffs, NJ, 1991).

Appendix

The dynamic equations of motion for a three joint modular robot operating in a horizontal plane are given by

$$D(q)\ddot{q} + C(q,\dot{q})\dot{q} + f(q,\dot{q}) = \tau \qquad (39)$$

where $D(q)$ is the 3×3 inertia matrix, $C(q,\dot{q})\dot{q}$ is the 3×1 vector of centrifugal and Coriolis torques, $f(q,\dot{q})$ is the 3×1 vector of frictional torques, and τ is the 3×1 vector of joint torques. The matrices are given as

$$D = \begin{bmatrix} D_{11} & D_{12} & D_{13} \\ D_{21} & D_{22} & D_{23} \\ D_{31} & D_{32} & D_{33} \end{bmatrix} \quad C = \begin{bmatrix} C_{11} & C_{12} & C_{13} \\ C_{21} & C_{22} & C_{23} \\ C_{31} & C_{32} & C_{33} \end{bmatrix}$$

$$F(q,\dot{q}) = \begin{bmatrix} f_1(q_1,\dot{q}_1) \\ f_2(q_2,\dot{q}_2) \\ f_3(q_3,\dot{q}_3) \end{bmatrix} \quad \tau = \begin{bmatrix} \tau_1 \\ \tau_2 \\ \tau_3 \end{bmatrix}$$

where

$$\begin{aligned} D_{11} &= I_1 + I_2 + I_3 + m_1 l_{c1}^2 + m_1 l_1^2 + m_2 l_{c2}^2 + m_3 l_1^2 \\ &\quad + m_3 l_2^2 + m_3 l_{c3}^2 + 2m_2 l_1 l_{c2} c_2 + 2m_3 l_1 l_2 c_2 \\ &\quad + 2m_3 l_1 l_2 c_2 + 2m_3 l_2 l_{c3} c_3 + 2m_3 l_1 l_{c3} c_{23} \\ D_{12} &= I_2 + I_3 + m_2 l_{c2}^2 + m_3 l_2^2 + m_3 l_{c3}^2 + m_2 l_1 l_{c2} c_2 \\ &\quad + 2m_3 l_2 l_{c3} c_3 + m_3 l_1 l_{c3} c_{23} \\ D_{21} &= D_{12} \\ D_{13} &= D_{31} = I_3 + m_3 l_{c3}^2 + m_3 l_2 l_{c3} c_3 + m_3 l_1 l_{c3} c_{23} \\ D_{22} &= I_2 + I_3 + m_2 l_{c2}^2 + m_3 l_2^2 + m_3 l_{c3}^2 + 2m_3 l_2 l_{c3} c_3 \end{aligned}$$

and $c_2 = \cos(q_2)$, $c_3 = \cos(q_3)$, $c_{23} = \cos(q_2 + q_3)$, $s_2 = \sin(q_2)$, $s_{23} = \sin(q_2 + q_3)$, m_i is the mass of ith link, l_i is the length of ith link, and l_{ci} is the distance from joint to the centre of mass of ith link, and I_i is the inertia of ith link. The link masses and inertias include both the actuator masses and actuator inertias.

The joint friction for the ith joint is modeled as

$$\begin{aligned} f_i(q_i,\dot{q}_i) &= \left(f_{ci} + f_{si}\exp\left(-f_{\tau i}\dot{q}_i^2\right)\right)\mathrm{sgn}(\dot{q}_i) \\ &\quad + b_i\dot{q}_i + f_{qi}(q_i,\dot{q}_i). \end{aligned}$$

The Coriolis matrix elements are given by

$$\begin{aligned} C_{11} &= c_{111}\dot{q}_1 + c_{112}\dot{q}_2 + c_{113}\dot{q}_3 \\ C_{12} &= c_{121}\dot{q}_1 + c_{122}\dot{q}_2 + c_{123}\dot{q}_3 \\ C_{13} &= c_{131}\dot{q}_1 + c_{132}\dot{q}_2 + c_{133}\dot{q}_3 \\ C_{21} &= c_{211}\dot{q}_1 + c_{212}\dot{q}_2 + c_{213}\dot{q}_3 \\ C_{22} &= c_{221}\dot{q}_1 + c_{222}\dot{q}_2 + c_{223}\dot{q}_3 \\ C_{23} &= c_{231}\dot{q}_1 + c_{232}\dot{q}_2 + c_{233}\dot{q}_3 \\ C_{31} &= c_{311}\dot{q}_1 + c_{312}\dot{q}_2 + c_{313}\dot{q}_3 \\ C_{32} &= c_{321}\dot{q}_1 + c_{322}\dot{q}_2 + c_{323}\dot{q}_3 \\ C_{33} &= c_{331}\dot{q}_1 + c_{332}\dot{q}_2 + c_{333}\dot{q}_3 \end{aligned}$$

https://doi.org/10.1017/S0263574707003608 Published online by Cambridge University Press

where

$$
\begin{aligned}
c_{111} &= 0 & c_{213} &= -m_3 l_2 l_{c3} s_3 \\
c_{112} &= -m_2 l_1 l_{c2} s_2 - m_3 l_1 l_{c2} s_2 & c_{231} &= c_{213} \\
&\quad - m_3 l_1 l_{c3} s_{23} & & \\
c_{121} &= c_{112} & c_{222} &= 0 \\
c_{113} &= -m_3 l_2 l_{c3} s_3 - m_3 l_1 l_{c3} s_{23} & c_{223} &= -m_3 l_2 l_{c3} s_3 \\
c_{131} &= c_{113} & c_{232} &= c_{223} \\
c_{122} &= -m_2 l_1 l_{c2} s_2 - m_3 l_1 l_2 s_2 & c_{233} &= -m_3 l_2 l_{c3} s_3 \\
&\quad - m_3 l_1 l_{c3} s_{23} & &
\end{aligned}
$$

$$
\begin{aligned}
c_{123} &= -m_3 l_2 l_{c3} s_3 - m_3 l_1 l_{c3} s_{23} & c_{312} &= m_3 l_2 l_{c3} s_3 \\
c_{132} &= c_{123} & &
\end{aligned}
$$

$$
\begin{aligned}
c_{133} &= -m_3 l_2 l_{c3} s_3 - m_3 l_1 l_{c3} s_{23} & c_{313} &= 0 \\
c_{211} &= m_3 l_1 l_2 s_2 + m_2 l_1 l_{c2} s_2 & c_{331} &= c_{313} \\
&\quad + m_3 l_1 l_{c3} s_{23} & & \\
c_{311} &= m_3 l_2 l_{c3} s_3 + m_3 l_1 l_{c3} s_{23} & c_{322} &= m_3 l_2 l_{c3} s_3 \\
c_{212} &= 0 & c_{323} &= 0 \\
c_{221} &= c_{212} & c_{332} &= c_{323} \\
c_{321} &= c_{312} & c_{333} &= 0.
\end{aligned}
$$

https://doi.org/10.1017/S0263574707003608 Published online by Cambridge University Press